



Nonlinear dynamic analysis of temperature-dependent functionally graded magnetostrictive sandwich nanobeams using different beam theories

A. H. Ghorbanpour-Arani¹ · M. Abdollahian² · A. Ghorbanpour Arani^{2,3}

Received: 26 November 2018 / Accepted: 4 May 2020 / Published online: 19 May 2020
© The Brazilian Society of Mechanical Sciences and Engineering 2020

Abstract

In the present study, nonlinear dynamic analysis of an embedded functionally graded sandwich nanobeam (FGSNB) integrated with magnetostrictive layers is investigated. The core layer of FGSNB, which is subjected to a time-dependent transverse load, is made of a two-constituent functionally graded material that the material properties of the functionally graded nanobeam are temperature dependent and assumed to vary in the thickness direction. The modified couple stress theory is taken into account so as to consider the small-scale effects. The surrounding elastic medium is simulated as visco-Pasternak foundation to study the effects of damping, shear and elastic effects of surrounded medium. Using energy method and Hamilton's principle, the governing motion equations and related boundary conditions are obtained for different beam theories. Finally, the differential quadrature as well as Newmark- β methods are employed to obtain the nonlinear dynamic response of the functionally graded magnetostrictive sandwich nanobeam (FGMSNB), and therefore deflection-response curves are plotted to study the effects of small-scale parameter, surrounding elastic medium, magnetostrictive layers, geometrical parameters, material compositions of core layer, environment temperature and boundary conditions and nonlinear terms graphically. The results indicate that the magnetostrictive layers play a key role on the dynamic behavior of the FGMSNB. Moreover, comparing results with those obtained in Ghorbanpour Arani and Abdollahian (Mech Adv Mater Struct, 2017. <https://doi.org/10.1080/15376494.2017.1387326>) shows the importance of the nonlinear terms. The obtained results in this paper can be used as sensor and actuator in the sensitive applications.

Keywords Nonlinear dynamic analysis · Magnetostrictive sandwich nanobeam · Functionally graded material · Modified couple stress theory · Visco-Pasternak medium

1 Introduction

Magnetostrictive materials are known as a type of smart materials that their size, shape and magnetization changes in response to the magnetic field and mechanical stress. Considering this fact, magnetostrictive materials can be used in

sensors and actuators applications. Therefore, many investigators have been selected magnetostrictive materials as a research topic. For instance, Wang and Lin [1] described the design of new giant magnetostrictive structures for double-nut ball screw pre-tightening. A magnetomechanical coupling constitutive relation of the giant magnetostrictive material was investigated experimentally and theoretically by Yongping et al. [2]. Sheikholeslami and Aghdam [3] investigated the bending behavior of magnetostrictive beam. Mishrar et al. [4] conducted the experiments in a thermal environment on Tb-Dy-Fe film samples to determine their characteristic magnetization curves. A three-variable plate model was utilized by Ebrahimi and Dabbagh [5] to explore the wave propagation problem of smart sandwich nanoplate made of a magnetostrictive core and ceramic face sheets while subjected to thermo-magnetic loading. A nonlinear constitutive model of a giant magnetostrictive actuator was

Technical Editor: Wallace Moreira Bessa, D.Sc.

✉ A. Ghorbanpour Arani
aghorban@kashanu.ac.ir; a_ghorbanpour@yahoo.com

¹ School of Mechanical Engineering, College of Engineering, University of Tehran, Tehran, Iran

² Faculty of Mechanical Engineering, University of Kashan, Kashan, Iran

³ Institute of Nanoscience and Nanotechnology, University of Kashan, Kashan, Iran

put forward for the application of effectively suppressing vibration by Zhang et al. [6]. Kumar et al. [5] analyzed the damping characteristics using distributed magnetostrictive layer bonded to an aluminum beam for different boundary conditions and coil configurations. They assumed that the magnetostrictive layer produces the actuating force required to control the vibration in the beam, based on a negative velocity feedback control law.

FGMs are innovative materials made of a combination of two material phases and can be classified as a recent improvement in composite materials. Due to this fact, FGMs are known as the materials with best properties and therefore can be applied in various fields such as the nuclear reactor and high-speed space craft industries. Numerous structural components of FGMs have beam-like configurations. Accordingly, investigating the buckling, vibration, dynamic response and wave propagation responses of FGM beams have been considered widely in the literature. Employing EBB theory and the physical neutral surface concept, the nonlinear governing equation for the FGM beam with two clamped ends and surface-bonded piezoelectric actuators was derived by the Hamilton's principle by Fu et al. [7]. Fallah and Aghdam [8] investigated the thermo-mechanical buckling and nonlinear free vibration analysis of FG beams on nonlinear elastic foundation. Analytical relations between the critical buckling load of a FGM TB and that of the corresponding EBB subjected to axial compressive load were derived by Li and Batra [9] for clamped-clamped (C-C), simply supported-simply supported (S-S) and Clamped-free (C-F) edges. Shen and Wang [10] studied the large amplitude vibration, nonlinear bending and thermal postbuckling of FGM beams resting on an elastic foundation in thermal environments.

Sandwich structures consist of a thick core integrated with two relatively thin face sheets in their simplest forms. Since the core layer is always thick and also light, and the face sheets are selected among the high rigidity, sandwich structures are applied in structures with high rigidity and low weight aerospace, airplanes, sensors and actuators. Recently, considerable amount of investigation has been reported on mechanical responses of sandwich structures by several researchers. Transient responses and natural frequencies of sandwich beams with inhomogeneous FG core were investigated by Bui et al. [11]. Vibration and thermal buckling behaviors of sandwich beams with composite facings and viscoelastic core were studied by Pradeep et al. [12]. Free vibration of the FG sandwich beams was studied by a mesh-free boundary-domain integral equation method by Yang et al. [13]. In another study, Vo et al. [14] presented finite element model for vibration and buckling of FG sandwich beams based on a refined shear deformation theory. They assumed that the core of sandwich beam is fully metal or ceramic and skins are composed of a FGM across the depth.

Recently, nanobeams are widely used in many nano- and micro-electromechanical systems (NEMS and MEMS) due to their unique mechanical, thermal and electronic properties. Owing to these properties, on the other hand, a large amount of researches have been carried out on the mechanical behavior of the functionally graded nanobeams (FGNBs). On the other hand, in order to study the mechanical characteristics of nanostructures accurately, size-dependent theories such as nonlocal elasticity, modified couple stress and modified strain gradient elasticity should be applied. Static bending and free vibration of FG microbeams were examined based on the MCST and various higher-order beam theories by Simsek and Reddy [15]. Nonlinear electromechanical behavior of nanobeams under electrostatic actuation based on the recently developed consistent couple stress theory was analyzed by Fakhrabadi and Yang [16]. Simsek [17] developed a non-classical beam theory for the static and nonlinear vibration analysis of microbeams based on a three-layered nonlinear elastic foundation within the framework of the MCST and EBB theory together with the von-Karman's geometric nonlinearity. Akgoz and Civalek [18] addressed the stability problem of micro-sized beam based on the strain gradient elasticity and modified couple stress theories.

The surrounded elastic medium of nanobeams can be assumed as Winkler, Pasternak and visco-Pasternak. The Winkler foundation is capable of just normal load while Pasternak foundation is both capable of transverse shear and normal loads. Among these simulation visco-Pasternak medium which considers damping, shear and normal loads can be assumed as an accurate model for surrounding elastic foundation. Ghorbanpour Arani and Shokravi [19] discussed vibration of coupled double-layer grapheme sheet systems coupled with each other by an enclosing visco-Pasternak medium. In another attempt, Ghorbanpour Arani et al. [20] analyzed the nonlinear dynamic stability of single-layered grapheme sheets (SLGSs) integrated with zinc oxide (ZnO) actuators and sensors embedded on visco-Pasternak foundation. Linear transient response of FG higher-order nanobeams integrated with magnetostrictive layers using modified couple stress theory was investigated by Ghorbanpour Arani and Abdollahian [21]. They assumed the visco-Pasternak elastic medium and studied the effects of damping, shear and spring modulus on the linear transient response of FG nanobeams.

Consequences of motivation, in this paper nonlinear dynamic analysis of an embedded FGSNB integrated with magnetostrictive layers is studied using MCST. The FGM-SNB is subjected to a time-dependent transverse load and the core is made of temperature-dependent FGM. Using the von-Karman nonlinear strain-displacement relationships and Hamilton's principle as well as energy method, the governing motion equations and related boundary

conditions are obtained for both EBB and TB models. The DQM in conjunction with Newmark- β method are applied to study the effects of small-scale parameter, geometrical parameters, surrounding elastic medium, magnetostrictive layers, material compositions of core layer, environment temperature and different boundary conditions.

2 Modified couple stress theory

Based on MCST, the strain energy density Π_s of a linear elastic material occupying region Ω with infinitesimal deformations can be expressed as [15, 22, 23]:

$$\Pi_s = \frac{1}{2} \int_{\Omega} (\sigma_{ij}\epsilon_{ij} + m_{ij}\chi_{ij}) d\Omega, \quad (i, j = 1, 2, 3), \quad (1)$$

where σ_{ij} is the Cauchy stress of sandwich nanobeam, ϵ_{ij} is the strain tensor, m_{ij} is the deviatoric part of the couple stress tensor and χ_{ij} is the symmetric curvature tensor where:

$$\epsilon_{ij} = \frac{1}{2} (u_{i,j} + u_{j,i}), \quad (2a)$$

$$\chi_{ij} = \frac{1}{2} (\theta_{i,j} + \theta_{j,i}), \quad (2b)$$

$$\theta_i = \frac{1}{2} e_{ijk} u_{k,j}, \quad (2c)$$

in which u_i , θ_i and e_{ijk} are the displacement vector, the infinitesimal rotation vector and the alternate tensor, respectively.

3 Governing motion equations

A uniform FGSNB with geometrical parameters of length L , width b , core thickness h_c and magnetostrictive layers thickness h_m is shown in Fig. 1. The nanobeam also embedded in visco-Pasternak medium and is subjected to time-dependent transverse load.

3.1 Preliminaries

The displacement components of an arbitrary point of the FGSNB in terms of x , y and z coordinates, denoted by $u_x(x, z, t)$, $u_y(x, z, t)$ and $u_z(x, z, t)$ is written as follows [15]:

$$u_x(x, z, t) = u(x, t) - z \frac{\partial w(x, t)}{\partial x} + \Phi(z)\gamma(x, t), \quad (3a)$$

$$u_y(x, z, t) = 0, \quad (3b)$$

$$u_z(x, z, t) = w(x, t). \quad (3c)$$

where $u(x, t)$ and $w(x, t)$ are the displacement components of the mid-plane in the axial and transverse directions, respectively. $\gamma(x, t)$ denotes the transverse shear strain of any point on the neutral axis which can be written as [15]:

$$\gamma(x, t) = \frac{\partial w(x, t)}{\partial x} - \phi(x, t), \quad (4)$$

where $\phi(x, t)$ is the total bending of the cross section at any point and t is time. For various beam models $\Phi(z)$ is defined as follows [15]:

- Euler–Bernoulli beam theory (EBBT): $\Phi(z) = 0$,
- First-order shear deformation beam theory (FSDBT): $\Phi(z) = z$,

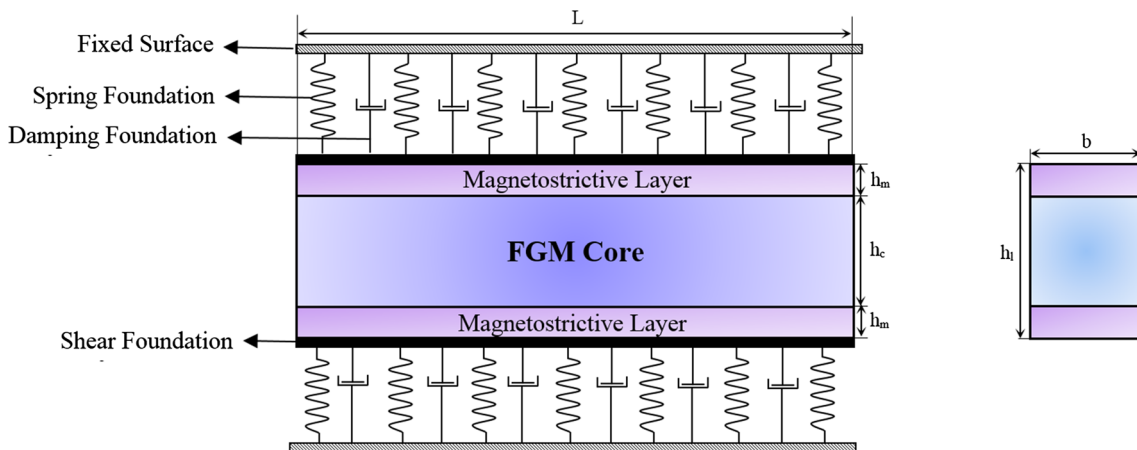


Fig. 1 Configuration of an embedded FGSMB

- Parabolic shear deformation beam theory (PSDBT): $\Phi(z) = z(1 - 4z^2/3h_l^2)$,
- Trigonometric shear deformation beam theory (TSDBT): $\Phi(z) = \frac{h_l}{\pi} \sin\left(\frac{\pi z}{h_l}\right)$,
- Hyperbolic shear deformation beam theory (HSDBT): $\Phi(z) = h_l \sinh\left(\frac{z}{h_l}\right) - z \cosh\left(\frac{1}{2}\right)$,
- Exponential shear deformation beam theory (ESDBT): $\Phi(z) = ze^{-2(z/h_l)^2}$.

Based on Eqs. (2a) and (3), the strain–displacement relations are obtained as:

$$\epsilon_{xx} = \frac{\partial u}{\partial x} - z \frac{\partial^2 w}{\partial x^2} + \frac{1}{2} \left(\frac{\partial w}{\partial x} \right)^2 + \Phi(z) \frac{\partial \gamma}{\partial x}, \epsilon_{yy} = \epsilon_{zz} = \epsilon_{xy} = \epsilon_{yz} = 0, \tag{5a}$$

$$\gamma_{xz} = 2\epsilon_{xz} = \frac{d\Phi(z)}{dz} \gamma. \tag{5b}$$

From Eqs. (2c) and (3), the components of rotation vector are obtained as follows:

$$\theta_x = 0, \tag{6a}$$

$$\theta_y = \frac{1}{2} \frac{d\Phi(z)}{dz} \gamma - \frac{\partial w}{\partial x}, \tag{6b}$$

$$\theta_z = 0. \tag{6c}$$

Considering Eqs. (2b) and (6) yields the nonzero components of symmetric curvature tensor as follows:

$$\chi_{xy} = \frac{1}{4} \frac{d\Phi(z)}{dz} \frac{\partial \gamma}{\partial x} - \frac{1}{2} \frac{\partial^2 w}{\partial x^2}, \tag{7a}$$

$$\chi_{yz} = \frac{1}{4} \frac{d^2\Phi(z)}{dz^2} \gamma. \tag{7b}$$

The nonzero components of stress tensor and deviatoric part of the couple stress for core and magnetostrictive layers, without considering the effect of thermal load, can be written as [23]:

$$\sigma_{xx}^c = Q_{11}^c \epsilon_{xx}, \tag{8a}$$

$$\sigma_{xz}^c = Q_{55}^c \gamma_{xz}, \tag{8b}$$

$$\sigma_{xx}^l = Q_{11}^l \epsilon_{xx} - e_{31} H_z, \tag{8c}$$

$$\sigma_{xz}^l = Q_{55}^l \gamma_{xz}, \tag{8d}$$

$$m_{xy}^c = 2Q_{55}^c l^2 \chi_{xy}, \tag{8e}$$

$$m_{yz}^c = 2Q_{55}^c l^2 \chi_{yz}, \tag{8f}$$

$$m_{xy}^l = 2Q_{55}^l l^2 \chi_{xy}, \tag{8g}$$

$$m_{yz}^l = 2Q_{55}^l l^2 \chi_{yz}, \tag{8h}$$

where l is the material length scale parameter, $Q_{ij}^i, i, j = 1, 2, \dots, 6$ are the elastic constants and the upper indexes l and c are related to magnetostrictive and core layers, respectively. Also:

$$Q_{11}^c = \frac{E}{1 - \nu^2}, \tag{9a}$$

$$Q_{55}^c = \frac{E}{2(1 + \nu)}, \tag{9b}$$

$$H_z = k_c c(t) \frac{\partial w}{\partial t}, \tag{9c}$$

in which E and ν are the Young’s modulus and Poisson’s ratio of the core, respectively. k_c is the coil constant and $c(t)$ denotes the control gain [6]. The Young’s modulus, Poisson’s ratio and density ρ_c of the FGM core can be expressed as [24]:

$$E = (E_2 - E_1) \left(\frac{2z + h_c}{2h_c} \right)^{V_f} + E_1, \tag{10a}$$

$$\nu = (\nu_2 - \nu_1) \left(\frac{2z + h_c}{2h_c} \right)^{V_f} + \nu_1, \tag{10b}$$

$$\rho_c = (\rho_{c2} - \rho_{c1}) \left(\frac{2z + h_c}{2h_c} \right)^{V_f} + \rho_{c1}, \tag{10c}$$

where E_2 and E_1 are the Young’s moduli, ν_2 and ν_1 are the Poisson’s ratio, ρ_{c2} and ρ_{c1} are the density of the constituent materials and V_f is the power law exponent, respectively [24]. Since most of FGMs are used in high-temperature applications, their properties must be assumed temperature dependent. Therefore, each property of the FGM core layer P_i is assumed to be the function of environment temperature $T(K)$, as follows [24]:

$$P_i = P_0 (P_{-1} T^{-1} + 1 + P_1 T + P_2 T^2 + P_3 T^3), \tag{11}$$

where P_0, P_{-1}, P_1, P_2 and P_3 are temperature coefficients of the constituent materials.

3.2 Strain energy of FGSNB

Substituting Eqs. (5) and (7) into Eq. (1) yields the variation of the FGSNB strain energy as follows:

$$\int_0^L \Pi_s dx = \int_0^L \left[N_x^t \left(\frac{\partial u}{\partial x} + \frac{1}{2} \left(\frac{\partial w}{\partial x} \right)^2 \right) - M_c^t \frac{\partial^2 w}{\partial x^2} + M_{nc}^t \frac{\partial \gamma}{\partial x} + Q_x^t \gamma + \frac{Y_2^t}{2} \frac{\partial \gamma}{\partial x} - Y_1^t \frac{\partial^2 w}{\partial x^2} + \frac{Y_3^t}{2} \gamma \right] dx, \tag{12}$$

where:

$$N_x^t = \int_{A_t} \sigma_{xx} dA_t = \int_{-h_i/2}^{-h_c/2} \sigma_{xx}^l b dz + \int_{-h_c/2}^{h_c/2} \sigma_{xx}^c b dz + \int_{h_c/2}^{h_i/2} \sigma_{xx}^l b dz, \tag{13a}$$

$$M_c^t = \int_{A_t} \sigma_{xx} z dA_t = \int_{-h_i/2}^{-h_c/2} \sigma_{xx}^l b z dz + \int_{-h_c/2}^{h_c/2} \sigma_{xx}^c b z dz + \int_{h_c/2}^{h_i/2} \sigma_{xx}^l b z dz, \tag{13b}$$

$$M_{nc}^t = \int_{A_t} \sigma_{xx} \Phi(z) dA_t = \int_{-h_i/2}^{-h_c/2} \sigma_{xx}^l \Phi(z) b dz + \int_{-h_c/2}^{h_c/2} \sigma_{xx}^c \Phi(z) b dz + \int_{h_c/2}^{h_i/2} \sigma_{xx}^l \Phi(z) b dz, \tag{13c}$$

$$Q_x^t = \int_{A_t} \sigma_{xz} \frac{d\Phi(z)}{dz} dA_t = \int_{-h_i/2}^{-h_c/2} \sigma_{xx}^l \frac{d\Phi(z)}{dz} b dz + \int_{-h_c/2}^{h_c/2} \sigma_{xx}^c \frac{d\Phi(z)}{dz} b dz + \int_{h_c/2}^{h_i/2} \sigma_{xx}^l \frac{d\Phi(z)}{dz} b dz, \tag{13d}$$

$$Y_1^t = \int_{A_t} m_{xy} dA_t = \int_{-h_i/2}^{-h_c/2} m_{xy}^l b dz + \int_{-h_c/2}^{h_c/2} m_{xy}^c b dz + \int_{h_c/2}^{h_i/2} m_{xy}^l b dz, \tag{13e}$$

$$Y_2^t = \int_{A_t} m_{xy} \frac{d\Phi(z)}{dz} dA_t = \int_{-h_i/2}^{-h_c/2} m_{xy}^l \frac{d\Phi(z)}{dz} b dz + \int_{-h_c/2}^{h_c/2} m_{xy}^c \frac{d\Phi(z)}{dz} b dz + \int_{h_c/2}^{h_i/2} m_{xy}^l \frac{d\Phi(z)}{dz} b dz, \tag{13f}$$

$$Y_3^t = \int_{A_t} m_{yz} \frac{d^2 \Phi(z)}{dz^2} dA_t = \int_{-h_i/2}^{-h_c/2} m_{yz}^l \frac{d^2 \Phi(z)}{dz^2} b dz + \int_{-h_c/2}^{h_c/2} m_{yz}^c \frac{d^2 \Phi(z)}{dz^2} b dz + \int_{h_c/2}^{h_i/2} m_{yz}^l \frac{d^2 \Phi(z)}{dz^2} b dz, \tag{13g}$$

where A_t is the total cross-sectional area of FGSNB. Equations (13) can be rewritten as follows using Eqs. (8):

$$N_x^t = A_{11} \frac{\partial u}{\partial x} - B_{11} \frac{\partial^2 w}{\partial x^2} + E_{11} \frac{\partial \gamma}{\partial x} + \frac{A_{11}}{2} \left(\frac{\partial w}{\partial x} \right)^2 - 2bh_L e_{31} k_c c(t) \frac{\partial w}{\partial t}, \tag{14a}$$

$$M_c^t = B_{11} \frac{\partial u}{\partial x} - D_{11} \frac{\partial^2 w}{\partial x^2} + F_{11} \frac{\partial \gamma}{\partial x} + \frac{B_{11}}{2} \left(\frac{\partial w}{\partial x} \right)^2, \tag{14b}$$

$$M_{nc}^t = E_{11} \frac{\partial u}{\partial x} - F_{11} \frac{\partial^2 w}{\partial x^2} + H_{11} \frac{\partial \gamma}{\partial x} + \frac{E_{11}}{2} \left(\frac{\partial w}{\partial x} \right)^2 - E_{31} k_c c(t) \frac{\partial w}{\partial t}, \tag{14c}$$

$$Q_x^t = B_{13} \gamma, \tag{14d}$$

$$Y_1^t = \frac{1}{2} D_{13} l^2 \frac{\partial \gamma}{\partial x} - A_{13} l^2 \frac{\partial^2 w}{\partial x^2}, \tag{14e}$$

$$Y_2^t = \frac{1}{2} B_{13} l^2 \frac{\partial \gamma}{\partial x} - D_{13} l^2 \frac{\partial^2 w}{\partial x^2}, \tag{14f}$$

$$Y_3^t = \frac{1}{2} E_{13} l^2 \gamma, \tag{14g}$$

where

$$(A_{11}, B_{11}, D_{11}) = \int_{-h_i/2}^{-h_c/2} Q_{11}^l(1, z, z^2) b dz + \int_{-h_c/2}^{h_c/2} Q_{11}^c(1, z, z^2) b dz + \int_{h_c/2}^{h_i/2} Q_{11}^l(1, z, z^2) b dz, \tag{15a}$$

$$(E_{11}, F_{11}, H_{11}) = \int_{-h_i/2}^{-h_c/2} Q_{11}^l \Phi(z)(1, z, z^2) b dz + \int_{-h_c/2}^{h_c/2} Q_{11}^c \Phi(z)(1, z, z^2) b dz + \int_{h_c/2}^{h_i/2} Q_{11}^l \Phi(z)(1, z, z^2) b dz, \tag{15b}$$

$$E_{31} = \int_{-h_1/2}^{-h_c/2} e_{31} \Phi(z) b dz + \int_{h_c/2}^{h_1/2} e_{31} \Phi(z) b dz, \tag{15c}$$

$$\begin{aligned} & (A_{13}, B_{13}, D_{13}, E_{13}) \\ &= \int_{-h_1/2}^{-h_c/2} Q'_{55} \left(1, \Phi_{,z}(z), [\Phi_{,z}(z)]^2, [\Phi_{,zz}(z)]^2 \right) b dz \\ &+ \int_{-h_c/2}^{h_c/2} Q'_{55} \left(1, \Phi_{,z}(z), [\Phi_{,z}(z)]^2, [\Phi_{,zz}(z)]^2 \right) b dz \\ &+ \int_{h_c/2}^{h_1/2} Q'_{55} \left(1, \Phi_{,z}(z), [\Phi_{,z}(z)]^2, [\Phi_{,zz}(z)]^2 \right) b dz, \end{aligned} \tag{15d}$$

3.3 Kinetic Energy of FGSNB

The kinetic energy of the FGSNB is written as [15]:

$$\begin{aligned} \Pi_k &= \frac{1}{2} \int_0^L \int_{-h_1/2}^{-h_c/2} \rho_l \left[\left(\frac{\partial u}{\partial t} - z \frac{\partial^2 w}{\partial x \partial t} + \Phi(z) \frac{\partial \gamma}{\partial t} \right)^2 + \left(\frac{\partial w}{\partial x} \right)^2 \right] b dz dx \\ &+ \frac{1}{2} \int_0^L \int_{-h_c/2}^{h_c/2} \rho_c(z) \left[\left(\frac{\partial u}{\partial t} - z \frac{\partial^2 w}{\partial x \partial t} + \Phi(z) \frac{\partial \gamma}{\partial t} \right)^2 + \left(\frac{\partial w}{\partial x} \right)^2 \right] b dz dx \\ &+ \frac{1}{2} \int_0^L \int_{h_c/2}^{h_1/2} \rho_l \left[\left(\frac{\partial u}{\partial t} - z \frac{\partial^2 w}{\partial x \partial t} + \Phi(z) \frac{\partial \gamma}{\partial t} \right)^2 + \left(\frac{\partial w}{\partial x} \right)^2 \right] b dz dx, \end{aligned} \tag{16}$$

where ρ_l are the density of magnetostrictive layers, respectively.

3.4 External forces

The total energy associated with external applied forces W_{ext} contains surrounding elastic medium and the distributed harmonically varying load f can be obtained as follows:

$$W_{ext} = \frac{1}{2} \int_0^T \int_0^L \left(f - k_w w + k_g \frac{\partial^2 w}{\partial x^2} - c_d \frac{\partial w}{\partial t} \right) w dx, \tag{17}$$

where k_w , k_g and c_d are spring, shear and damping modulus, respectively, and:

$$f(x, t) = f_0 \sin \left(\frac{n\pi x}{L} \right) e^{\alpha t}, \tag{18}$$

in which f_0 is a constant, α is an integer and ω is the frequency of variation of the load [25].

3.5 Hamilton's principle

Hamilton's principle on the interval time $[0, T]$ is defined as:

$$\delta \int_0^T (\Pi_k - \Pi_s + W_{ext}) dt = 0, \tag{19}$$

Substituting Eqs. (12), (16) and (17) into Eq. (19), integrating by parts and setting the coefficients of δu , δw and $\delta \gamma$ to zero yields the motion equations of the FGSNB as follows

$$\delta u : \frac{\partial N'_x}{\partial x} = I_A \frac{\partial^2 u}{\partial t^2} - I_B \frac{\partial^3 w}{\partial x \partial t^2} + I_E \frac{\partial^2 \gamma}{\partial t^2}, \tag{20a}$$

$$\begin{aligned} \delta w : \frac{\partial}{\partial x} \left(N'_x \frac{\partial w}{\partial x} \right) + \frac{\partial^2 M'_c}{\partial x^2} + \frac{\partial^2 Y'_1}{\partial x^2} + f - k_w w + k_g \frac{\partial^2 w}{\partial x^2} - c_d \frac{\partial w}{\partial t} \\ = I_A \frac{\partial^2 w}{\partial t^2} + I_B \frac{\partial^3 u}{\partial x \partial t^2} - I_D \frac{\partial^4 w}{\partial x^2 \partial t^2} + I_F \frac{\partial^3 \gamma}{\partial x \partial t^2}, \end{aligned} \tag{20b}$$

$$\delta \gamma : \frac{\partial M'_{nc}}{\partial x} - Q'_x + \frac{1}{2} \frac{\partial Y'_2}{\partial x} - \frac{1}{2} Y'_3 = I_E \frac{\partial^2 u}{\partial t^2} - I_F \frac{\partial^3 w}{\partial x \partial t^2} + I_H \frac{\partial^2 \gamma}{\partial t^2}. \tag{20c}$$

where

$$\begin{aligned} (I_A, I_B, I_D) &= \int_{-h_1/2}^{-h_c/2} \rho_l(z) (1, z, z^2) b dz \\ &+ \int_{-h_c/2}^{h_c/2} \rho_c(z) (1, z, z^2) b dz + \int_{h_c/2}^{h_1/2} \rho_l(z) (1, z, z^2) b dz, \end{aligned} \tag{21a}$$

$$\begin{aligned} (I_E, I_F, I_H) &= \int_{-h_1/2}^{-h_c/2} \rho_l(z) \Phi(z) (1, z, \Phi(z)) b dz \\ &+ \int_{-h_c/2}^{h_c/2} \rho_c(z) \Phi(z) (1, z, \Phi(z)) b dz \\ &+ \int_{h_c/2}^{h_1/2} \rho_l(z) \Phi(z) (1, z, \Phi(z)) b dz, \end{aligned} \tag{21b}$$

And the related boundary conditions are obtained as:

$$x = 0, L : u = 0 \text{ OR } N'_x = 0, \tag{22a} \quad x = 0, L : \frac{\partial w}{\partial x} = 0 \text{ OR } M'_c + Y'_1 = 0, \tag{22c}$$

$$x = 0, L : w = 0 \text{ OR } I_B \frac{\partial^2 u}{\partial t^2} - I_D \frac{\partial^3 w}{\partial x \partial t^2} + I_F \frac{\partial^2 \gamma}{\partial t^2} - N'_x \frac{\partial w}{\partial x} - \frac{\partial M'_c}{\partial x} - \frac{\partial Y'_1}{\partial x} = 0, \tag{22b} \quad x = 0, L : \gamma = 0 \text{ OR } M'_{nc} + \frac{1}{2} Y'_2 = 0. \tag{22d}$$

It is worth mentioning that the initial displacements and the initial velocities of the beam are assumed to be zero [25].

It is convenient to introduce the following dimensionless parameters as:

$$X = \frac{x}{L}, (U, W) = \left(\frac{u}{h}, \frac{w}{h} \right), l_0 = \frac{l}{h}, \eta = \frac{h}{L}, \Gamma = \gamma, T = \frac{t}{L} \sqrt{\frac{A_{11}}{I_A}}, \Omega = \omega L \sqrt{\frac{I_A}{A_{11}}},$$

$$(\bar{B}_{11}, \bar{D}_{11}, \bar{E}_{11}, \bar{F}_{11}, \bar{H}_{11}) = \left(\frac{B_{11}}{A_{11}L}, \frac{D_{11}}{A_{11}L^2}, \frac{E_{11}}{A_{11}h}, \frac{F_{11}}{A_{11}h^2}, \frac{H_{11}}{A_{11}h^2} \right), M_{31} = \frac{2bhLe_{31}k_c c(t)}{\sqrt{I_A A_{11}}}, \tag{23}$$

$$M_{32} = \frac{E_{31}k_c c(t)}{h\sqrt{I_A A_{11}}}, (\bar{I}_B, \bar{I}_D, \bar{I}_E, \bar{I}_F, \bar{I}_H) = \left(\frac{I_B}{I_A L}, \frac{I_D}{I_A L^2}, \frac{I_E}{I_A h}, \frac{I_F}{I_A h^2}, \frac{I_H}{I_A h^2} \right), \alpha_T = L \sqrt{\frac{I_A}{A_{11}}},$$

$$(\bar{A}_{13}, \bar{D}_{13}, \bar{B}_{13}, \bar{E}_{13}) = \left(\frac{A_{13}}{A_{11}}, \frac{D_{13}}{A_{11}}, \frac{B_{13}}{A_{11}}, \frac{E_{13}L^2}{A_{11}} \right), K_c = \frac{c_d L}{\sqrt{I_A A_{11}}}, K_w = \frac{k_w L^2}{A_{11}}, K_g = \frac{k_g}{A_{11}}, F_0 = \frac{f_0 L^2}{A_{11} h}.$$

Substituting Eqs. (14) into Eqs. (20) and (22) and using Eqs. (23), the dimensionless governing motion equations are derived as follows:

$$\frac{\partial^2 U}{\partial X^2} - \bar{B}_{11} \frac{\partial^3 W}{\partial X^3} + \bar{E}_{11} \frac{\partial^2 \Gamma}{\partial X^2} + \eta \frac{\partial W}{\partial X} \frac{\partial^2 W}{\partial X^2} - M_{31} \frac{\partial^2 W}{\partial X \partial T} = \frac{\partial^2 U}{\partial T^2} - \bar{I}_B \frac{\partial^3 W}{\partial X \partial T^2} + \bar{I}_E \frac{\partial^2 \Gamma}{\partial T^2}, \tag{24a}$$

$$\eta \frac{\partial^2 U}{\partial X^2} \frac{\partial W}{\partial X} + \bar{E}_{11} \eta \frac{\partial W}{\partial X} \frac{\partial^2 \Gamma}{\partial X^2} + \frac{3\eta^2}{2} \left(\frac{\partial W}{\partial X} \right)^2 \frac{\partial^2 W}{\partial X^2} - M_{31} \eta \frac{\partial^2 W}{\partial X \partial T} \frac{\partial W}{\partial X}$$

$$+ \eta \frac{\partial U}{\partial X} \frac{\partial^2 W}{\partial X^2} + \bar{E}_{11} \eta \frac{\partial \Gamma}{\partial X} \frac{\partial^2 W}{\partial X^2} - M_{31} \eta \frac{\partial W}{\partial \tau} \frac{\partial^2 W}{\partial X^2} + \bar{B}_{11} \frac{\partial^3 U}{\partial X^3} - \bar{D}_{11} \frac{\partial^4 W}{\partial X^4}$$

$$+ \bar{F}_{11} \eta \frac{\partial^3 \Gamma}{\partial X^3} + \frac{1}{2} \bar{B}_{13} \eta l_0^2 \frac{\partial^3 \Gamma}{\partial X^3} - \bar{A}_{13} l_0^2 \eta^2 \frac{\partial^4 W}{\partial X^4} + F_0 \sin(\Omega T) e^{\alpha_T T}$$

$$- K_w W + K_g \frac{\partial^2 W}{\partial X^2} - K_c \frac{\partial W}{\partial T} = \frac{\partial^2 W}{\partial T^2} + \bar{I}_B \frac{\partial^3 U}{\partial X \partial T^2} - \bar{I}_D \frac{\partial^4 W}{\partial X^2 \partial T^2} + \bar{I}_F \eta \frac{\partial^3 \Gamma}{\partial X \partial T^2}, \tag{24b}$$

$$\bar{E}_{11} \frac{\partial^2 U}{\partial X^2} - \bar{F}_{11} \eta \frac{\partial^3 W}{\partial X^3} + \bar{H}_{11} \frac{\partial^2 \Gamma}{\partial X^2} + \bar{E}_{11} \eta \frac{\partial W}{\partial X} \frac{\partial^2 W}{\partial X^2} - M_{32} \frac{\partial^2 W}{\partial X \partial T} - \frac{\bar{D}_{13}}{\eta^2} \Gamma + \frac{1}{4} \bar{D}_{13} l_0^2 \frac{\partial^2 \Gamma}{\partial X^2}$$

$$- \frac{1}{2} \bar{B}_{13} l_0^2 \eta \frac{\partial^3 W}{\partial X^3} - \frac{1}{4} \bar{E}_{13} l_0^2 \Gamma = \bar{I}_E \frac{\partial^2 U}{\partial T^2} - \bar{I}_F \eta \frac{\partial^3 W}{\partial X \partial T^2} + \bar{I}_H \frac{\partial^2 \Gamma}{\partial T^2}. \tag{24c}$$

And dimensionless boundary conditions are obtained as follows:

$$X = 0, L : U = 0 \text{ OR } \frac{\partial U}{\partial X} - \bar{B}_{11} \frac{\partial^2 W}{\partial X^2} + \bar{E}_{11} \frac{\partial \Gamma}{\partial X} + \frac{\eta}{2} \left(\frac{\partial W}{\partial X} \right)^2 - M_{31} \frac{\partial W}{\partial T} = 0, \tag{25a}$$

$$\begin{aligned}
 X = 0, L : \quad W = 0 \quad \text{OR} \quad & \bar{I}_B \frac{\partial^2 U}{\partial T^2} - \bar{I}_D \frac{\partial^3 W}{\partial X \partial T^2} + \bar{I}_F \eta \frac{\partial^2 \Gamma}{\partial T^2} + \eta \frac{\partial U}{\partial X} \frac{\partial W}{\partial X} - \bar{B}_{11} \eta \frac{\partial^2 W}{\partial X^2} \frac{\partial W}{\partial X} \\
 & + \bar{E}_{11} \eta \frac{\partial \Gamma}{\partial X} \frac{\partial W}{\partial X} + \frac{\eta^2}{2} \left(\frac{\partial W}{\partial X} \right)^2 \frac{\partial W}{\partial X} - M_{31} \frac{\partial W}{\partial \tau} \frac{\partial W}{\partial X} - \bar{B}_{11} \frac{\partial^2 U}{\partial X^2} \\
 & + \bar{D}_{11} \frac{\partial^3 W}{\partial X^3} - \bar{F}_{11} \eta \frac{\partial^2 \Gamma}{\partial X^2} - \bar{B}_{11} \eta \frac{\partial W}{\partial X} \frac{\partial^2 W}{\partial X^2} - \frac{1}{2} \bar{B}_{13} l_0^2 \eta \frac{\partial^2 \Gamma}{\partial X^2} \\
 & + \bar{A}_{13} l_0^2 \eta^2 \frac{\partial^3 W}{\partial X^3} - K_g \frac{\partial W}{\partial X} = 0,
 \end{aligned} \tag{25b}$$

$$\begin{aligned}
 X = 0, L : \quad \frac{\partial W}{\partial X} = 0 \quad \text{OR} \quad & \bar{B}_{11} \frac{\partial U}{\partial X} - \bar{D}_{11} \frac{\partial^2 W}{\partial X^2} + \bar{F}_{11} \eta \frac{\partial \Gamma}{\partial X} + \frac{1}{2} \bar{B}_{13} l_0^2 \eta \frac{\partial \Gamma}{\partial X} - \bar{A}_{13} l_0^2 \eta^2 \frac{\partial^2 W}{\partial X^2} \\
 & + \frac{\bar{B}_{11}}{2} \eta \left(\frac{\partial W}{\partial X} \right)^2 = 0,
 \end{aligned} \tag{25c}$$

$$\begin{aligned}
 X = 0, L : \quad \Gamma = 0 \quad \text{OR} \quad & \bar{E}_{11} \frac{\partial U}{\partial X} - \bar{F}_{11} \eta \frac{\partial^2 W}{\partial X^2} + \bar{H}_{11} \frac{\partial \Gamma}{\partial X} - M_{32} \frac{\partial W}{\partial T} + \frac{1}{4} \bar{D}_{13} l_0^2 \frac{\partial \Gamma}{\partial X} \\
 & + \frac{\bar{E}_{11}}{2} \eta \left(\frac{\partial W}{\partial X} \right)^2 - \frac{1}{2} \bar{B}_{13} l_0^2 \eta \frac{\partial^2 W}{\partial X^2} = 0.
 \end{aligned} \tag{25d}$$

Therefore, for simply supported end conditions, one can write the following expression:

$$\begin{aligned}
 U = 0, W = 0, \bar{B}_{11} \frac{\partial U}{\partial X} - \bar{D}_{11} \frac{\partial^2 W}{\partial X^2} + \bar{F}_{11} \eta \frac{\partial \Gamma}{\partial X} + \frac{1}{2} \bar{B}_{13} l_0^2 \eta \frac{\partial \Gamma}{\partial X} - \bar{A}_{13} l_0^2 \eta^2 \frac{\partial^2 W}{\partial X^2} + \frac{\bar{B}_{11}}{2} \eta \left(\frac{\partial W}{\partial X} \right)^2 &= 0, \\
 \bar{E}_{11} \frac{\partial U}{\partial X} - \bar{F}_{11} \eta \frac{\partial^2 W}{\partial X^2} + \bar{H}_{11} \frac{\partial \Gamma}{\partial X} - M_{32} \frac{\partial W}{\partial T} + \frac{1}{4} \bar{D}_{13} l_0^2 \frac{\partial \Gamma}{\partial X} + \frac{\bar{E}_{11}}{2} \eta \left(\frac{\partial W}{\partial X} \right)^2 - \frac{1}{2} \bar{B}_{13} l_0^2 \eta \frac{\partial^2 W}{\partial X^2} &= 0.
 \end{aligned} \tag{26}$$

And for clamped end conditions:

$$U = 0, W = 0, \frac{\partial W}{\partial X} = 0, \Gamma = 0. \tag{27}$$

U, W and Γ and their derivatives with respect to X can be expressed as [22, 26]:

$$\{U, W, \Gamma\} = \sum_{m=1}^N l_m(X) \{U_m(X_m, t), W_m(X_m, t), \Gamma_m(X_m, t)\}, \tag{28a}$$

4 Solution method

In the present study, the DQM in conjunction with Newmark- β are employed to solve the governing motion equations. For this purpose, first, the DQM is applied. The main idea of this method is that the partial derivative of a function with respect to spatial variables at a given discrete point is approximated as a weighted linear sum of the function values at all discrete points chosen in the solution domain. Therefore, the functions

$$\frac{\partial^k}{\partial X^k} \{U, W, \Gamma\} \Big|_{X=X_i} = \sum_{m=1}^N C_{im}^{(k)}(X) \{U_m(X_m, t), W_m(X_m, t), \Gamma_m(X_m, t)\}, \tag{28b}$$

where N is the total number of grid points along X , $l_m(X)$ is the Lagrange interpolation polynomials and $C_{im}^{(k)}$ represents the weighting coefficients, which can be found in [22, 26]. The Chebyshev polynomials are chosen for the positions of the grid points which can be expressed as:

$$X_i = \frac{1}{2} \left(1 - \cos \left(\frac{\pi(i-1)}{N-1} \right) \right), \quad i = 1, 2, \dots, N \quad (29)$$

Substituting Eqs. (28) into Eqs. (24) yields the following differential equations as:

$$\begin{aligned} & \sum_{m=1}^N C_{im}^{(2)} U_m - \bar{B}_{11} \sum_{m=1}^N C_{im}^{(3)} W_m + \bar{E}_{11} \sum_{m=1}^N C_{im}^{(2)} \Gamma_m + \eta \sum_{m=1}^N C_{im}^{(1)} W_m \sum_{m=1}^N C_{im}^{(2)} W_m \\ & - M_{31} \sum_{m=1}^N C_{im}^{(1)} \dot{W}_m = \ddot{U}_i - \bar{I}_B \sum_{m=1}^N C_{im}^{(1)} \ddot{W}_m + \bar{I}_E \ddot{\Gamma}_i, \end{aligned} \quad (30a)$$

$$\begin{aligned} & \eta \sum_{m=1}^N C_{im}^{(2)} U_m \sum_{m=1}^N C_{im}^{(1)} W_m + \bar{E}_{11} \eta \sum_{m=1}^N C_{im}^{(1)} W_m \sum_{m=1}^N C_{im}^{(2)} \Gamma_m + \frac{3\eta^2}{2} \left(\sum_{m=1}^N C_{im}^{(1)} W_m \right)^2 \sum_{m=1}^N C_{im}^{(2)} W_m \\ & - M_{31} \eta \sum_{m=1}^N C_{im}^{(1)} \dot{W}_m \sum_{m=1}^N C_{im}^{(1)} W_m + \eta \sum_{m=1}^N C_{im}^{(1)} U_m \sum_{m=1}^N C_{im}^{(2)} W_m + \bar{E}_{11} \eta \sum_{m=1}^N C_{im}^{(2)} W_m \sum_{m=1}^N C_{im}^{(1)} \Gamma_m \\ & - M_{31} \eta \dot{W}_i \sum_{m=1}^N C_{im}^{(2)} W_m + \bar{B}_{11} \sum_{m=1}^N C_{im}^{(3)} U_m - \bar{D}_{11} \sum_{m=1}^N C_{im}^{(4)} W_m + \bar{F}_{11} \eta \sum_{m=1}^N C_{im}^{(3)} \Gamma_m \\ & + \frac{1}{2} \bar{B}_{13} \eta l_0^2 \sum_{m=1}^N C_{im}^{(3)} \Gamma_m - \bar{A}_{13} l_0^2 \eta^2 \sum_{m=1}^N C_{im}^{(4)} W_m + F_0 \sin(\Omega T) e^{\alpha_r T} - K_w W_i \\ & + K_g \sum_{m=1}^N C_{im}^{(2)} W_m - K_c \dot{W}_i = \ddot{W}_i + \bar{I}_B \sum_{m=1}^N C_{im}^{(1)} \ddot{U}_m - \bar{I}_D \sum_{m=1}^N C_{im}^{(2)} \ddot{W}_m + \bar{I}_F \eta \sum_{m=1}^N C_{im}^{(1)} \ddot{\Gamma}_m, \end{aligned} \quad (30b)$$

$$\begin{aligned} & \bar{E}_{11} \sum_{m=1}^N C_{im}^{(2)} U_m - \bar{F}_{11} \eta \sum_{m=1}^N C_{im}^{(3)} W_m + \bar{H}_{11} \sum_{m=1}^N C_{im}^{(2)} \Gamma_m + \bar{E}_{11} \eta \sum_{m=1}^N C_{im}^{(1)} W_m \sum_{m=1}^N C_{im}^{(2)} W_m \\ & - M_{32} \sum_{m=1}^N C_{im}^{(1)} \dot{W}_m - \frac{\bar{B}_{13}}{\eta^2} \Gamma_i + \frac{1}{4} \bar{B}_{13} l_0^2 \sum_{m=1}^N C_{im}^{(2)} \Gamma_m - \frac{1}{2} \bar{D}_{13} l_0^2 \eta \sum_{m=1}^N C_{im}^{(3)} W_m - \frac{1}{4} \bar{E}_{13} l_0^2 \Gamma \\ & = \bar{I}_E \ddot{U}_i - \bar{I}_F \eta \sum_{m=1}^N C_{im}^{(1)} \ddot{W}_m + \bar{I}_H \ddot{\Gamma}_i. \end{aligned} \quad (30c)$$

where the over dot indicates the partial derivatives with respect to the dimensionless time. Also, inserting Eqs. (28) into Eqs. (26) and (27) yields the following equations for C–C, S–S and clamped–simply supported (C–S) boundary conditions as:

$$\begin{aligned} \text{C–C : } & U_1 = 0, W_1 = 0, \sum_{m=1}^N C_{1m}^{(1)} W_m = 0, \Gamma_1 = 0, \quad \text{at } X = 0, \\ & U_N = 0, W_N = 0, \sum_{m=1}^N C_{Nm}^{(1)} W_m = 0, \Gamma_N = 0, \quad \text{at } X = 1 \end{aligned} \quad (31a)$$

S - S : $U_1 = 0, W_1 = 0,$

$$\begin{aligned} & \bar{B}_{11} \sum_{m=1}^N C_{1m}^{(1)} U_m - \bar{D}_{11} \sum_{m=1}^N C_{1m}^{(2)} W_m + \bar{F}_{11} \eta \sum_{m=1}^N C_{1m}^{(1)} \Gamma_m + \frac{1}{2} \bar{B}_{13} l_0^2 \eta \sum_{m=1}^N C_{1m}^{(1)} \Gamma_m \\ & - \bar{A}_{13} l_0^2 \eta^2 \sum_{m=1}^N C_{1m}^{(2)} W_m + \frac{\bar{B}_{11}}{2} \eta \left(\sum_{m=1}^N C_{1m}^{(1)} W_m \right)^2 = 0, \\ & \bar{E}_{11} \sum_{m=1}^N C_{1m}^{(1)} U_m - \bar{F}_{11} \eta \sum_{m=1}^N C_{1m}^{(2)} W_m + \bar{H}_{11} \sum_{m=1}^N C_{1m}^{(1)} \Gamma_m - M_{32} \dot{W}_1 + \frac{1}{4} \bar{D}_{13} l_0^2 \sum_{m=1}^N C_{1m}^{(1)} \Gamma_m \\ & + \frac{\bar{E}_{11}}{2} \eta \left(\sum_{m=1}^N C_{1m}^{(1)} W_m \right)^2 - \frac{1}{2} \bar{B}_{13} l_0^2 \eta \sum_{m=1}^N C_{1m}^{(2)} W_m = 0. \quad \text{at } X = 0, \end{aligned} \tag{31b}$$

$U_N = 0, W_N = 0,$

$$\begin{aligned} & \bar{B}_{11} \sum_{m=1}^N C_{Nm}^{(1)} U_m - \bar{D}_{11} \sum_{m=1}^N C_{Nm}^{(2)} W_m + \bar{F}_{11} \eta \sum_{m=1}^N C_{Nm}^{(1)} \Gamma_m + \frac{1}{2} \bar{B}_{13} l_0^2 \eta \sum_{m=1}^N C_{Nm}^{(1)} \Gamma_m \\ & - \bar{A}_{13} l_0^2 \eta^2 \sum_{m=1}^N C_{Nm}^{(2)} W_m + \frac{\bar{B}_{11}}{2} \eta \left(\sum_{m=1}^N C_{Nm}^{(1)} W_m \right)^2 = 0, \\ & \bar{E}_{11} \sum_{m=1}^N C_{Nm}^{(1)} U_m - \bar{F}_{11} \eta \sum_{m=1}^N C_{Nm}^{(2)} W_m + \bar{H}_{11} \sum_{m=1}^N C_{Nm}^{(1)} \Gamma_m - M_{32} \dot{W}_N + \frac{1}{4} \bar{D}_{13} l_0^2 \sum_{m=1}^N C_{Nm}^{(1)} \Gamma_m \\ & + \frac{\bar{E}_{11}}{2} \eta \left(\sum_{m=1}^N C_{Nm}^{(1)} W_m \right)^2 - \frac{1}{2} \bar{B}_{13} l_0^2 \eta \sum_{m=1}^N C_{Nm}^{(2)} W_m = 0. \quad \text{at } X = 1, \end{aligned}$$

C - S : $U_1 = 0, W_1 = 0, \sum_{m=1}^N C_{1m}^{(1)} W_m = 0, \Gamma_1 = 0, \quad \text{at } X = 0,$

$U_N = 0, W_N = 0,$

$$\begin{aligned} & \bar{B}_{11} \sum_{m=1}^N C_{Nm}^{(1)} U_m - \bar{D}_{11} \sum_{m=1}^N C_{Nm}^{(2)} W_m + \bar{F}_{11} \eta \sum_{m=1}^N C_{Nm}^{(1)} \Gamma_m + \frac{1}{2} \bar{B}_{13} l_0^2 \eta \sum_{m=1}^N C_{Nm}^{(1)} \Gamma_m \\ & - \bar{A}_{13} l_0^2 \eta^2 \sum_{m=1}^N C_{Nm}^{(2)} W_m + \frac{\bar{B}_{11}}{2} \eta \left(\sum_{m=1}^N C_{Nm}^{(1)} W_m \right)^2 = 0, \end{aligned} \tag{31c}$$

$$\begin{aligned} & \bar{E}_{11} \sum_{m=1}^N C_{Nm}^{(1)} U_m - \bar{F}_{11} \eta \sum_{m=1}^N C_{Nm}^{(2)} W_m + \bar{H}_{11} \sum_{m=1}^N C_{Nm}^{(1)} \Gamma_m - M_{32} \dot{W}_N + \frac{1}{4} \bar{D}_{13} l_0^2 \sum_{m=1}^N C_{Nm}^{(1)} \Gamma_m \\ & + \frac{\bar{E}_{11}}{2} \eta \left(\sum_{m=1}^N C_{Nm}^{(1)} W_m \right)^2 - \frac{1}{2} \bar{B}_{13} l_0^2 \eta \sum_{m=1}^N C_{Nm}^{(2)} W_m = 0. \quad \text{at } X = 1, \end{aligned}$$

Considering Eqs. (30) and (31) and explanations presented in “Appendix”, the governing motion equations can be obtained as follows:

$$[M]\{\ddot{d}\}_d + [C_{NL} + C_L]\{\dot{d}\}_d + [K_{NL} + K_L]\{d\}_d = \{F\}, \tag{32}$$

5 Numerical results and discussion

In this study based on the DQM for space discretization and Newmark-β method for time discretization, the nonlinear dynamic response of the embedded FGMSNB is obtained

$$W|_{x=0.5} = \frac{F_0}{\bar{D}_{11}(\pi^4 - \Omega^2)} \left(\sin(\Omega T) - \left(\frac{\Omega}{\pi^2 \sqrt{\bar{D}_{11}}} \right) \sin\left(\pi^2 \sqrt{\bar{D}_{11}} T\right) \right) \tag{33}$$

for C–C, S–S and C–S boundary conditions. The sandwich nanobeam consists of a FGM core integrated with magnetostrictive layers. The temperature-dependent material properties of FGM constituent materials which are taken from Ref. [24] are listed in Table 1.

It should be noted that in the present study, the room temperature ($T = 25 \text{ }^\circ\text{C}$) is assumed to calculate the material properties in Eq. (11). Also, the Young’s modulus for Terfenol-D magnetostrictive layer is $E = 26.5 \text{ GPa}$ and the magnetostrictive coupling moduli are $e_{31} = e_{32} = E^m d^m$ where $E^m = 26.5 \text{ GPa}$, $d^m = 1.67 \times 10^{-8} \text{ m/A}$ [6]. Moreover, the following data used for geometry of the FGMSNB and elastic medium constants: the core thickness $h_c = 1 \text{ (nm)}$, the thickness of each magnetostrictive layer $h_m = 0.25 \text{ (nm)}$, the aspect ratio of length to the thickness $L/h_l = 8$, the spring constant of elastic medium $k_w = 100 \text{ (MN/m}^2\text{)}$, the shear constant of elastic medium $k_g = 1 \text{ (nN)}$ and the damping modulus constant of elastic foundation $k_c = 3 \times 10^{-4} \text{ (kg/ms)}$. Also the external harmonic load properties used for the presented results are $F_0 = 0.5$ and $\alpha_T = -0.1$.

5.1 Validation

In order to check the validity and accuracy of the presented solution, the linear results are compared with the exact solution obtained by Rao [25]. Using Eqs. (23), the dimensionless midpoint displacement for the S–S EBBT beam subjected to a harmonically varying load as $F_0 \sin(\Omega T) \sin(n\pi X)$ is obtained as [25]:

Figure 2a and b compares the dimensionless midpoint deflection of the S–S EBB FGMSNB obtained with the DQM in conjunction with Newmark-β method with the exact solution obtained in Eq. (33) and good agreement can be seen between them.

5.2 Convergence of numerical solution

In order to check the convergence and accuracy of the DQM, the appropriate number of grid points is obtained. For this purpose, the maximum dimensionless midpoint deflections ($W|_{x=0.5}$) of the FGSNB for different values of grid points for both linear and nonlinear analysis are presented in Tables 2, 3 and 4 for C–C, C–S and S–S boundary conditions, respectively. As can be seen, the maximum dimensionless midpoint deflection values are converged for $N = 15$, $N = 19$ and $N = 13$ for C–C, C–S and S–S boundary conditions, respectively.

From Tables 2, 3 and 4, it can be found that results obtained from different theories are close to each other. Therefore from here to the end of the manuscript in order to obtain the results, PSDBT is chosen.

Table 1 Material properties of the FGM core [24]

	Stainless steel		Nickel	
	Density (kg/m ³)			
	7900		8909	
Coefficient	$E \text{ (N/m}^2\text{)}$	ν	$E \text{ (N/m}^2\text{)}$	ν
P_0	201.04×10^9	0.3262	244.27×10^9	0.2882
P_{-1}	0	0	0	0
P_1	3.079×10^{-4}	2.002×10^{-4}	-1.371×10^{-4}	1.133×10^{-4}
P_2	-6.534×10^{-7}	3.797×10^{-7}	1.214×10^{-7}	0
P_3	0	0	-3.681×10^{-7}	0

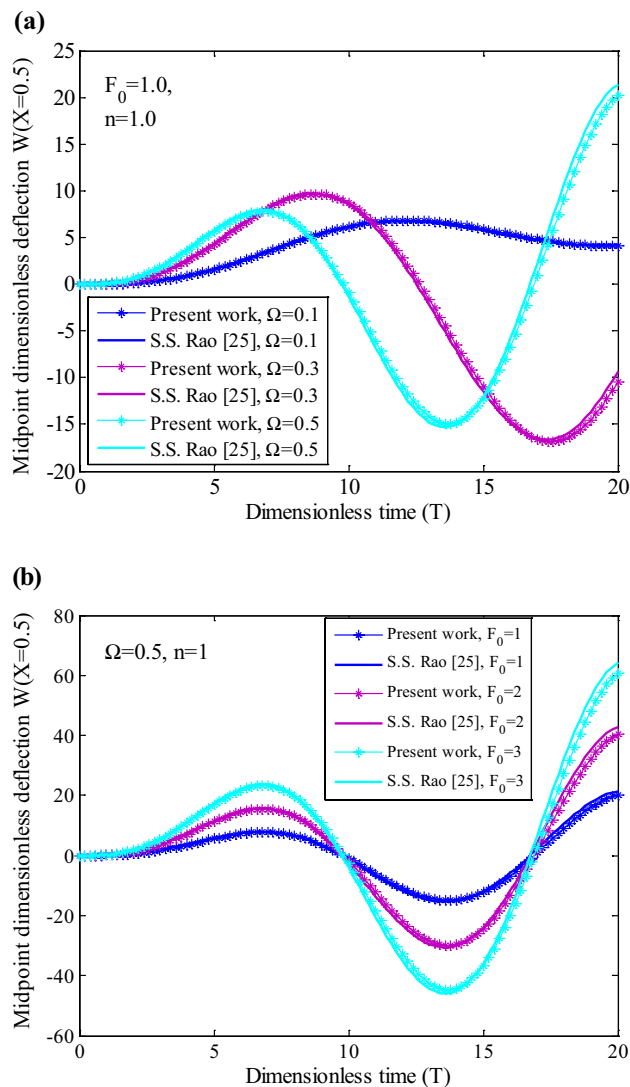


Fig. 2 Dimensionless midpoint deflection of the S–S EBB FGMSNB obtained from the presented method and exact solution [23] **a** $F_0 = 1.0$, $n = 1.0$ and **b** $\Omega = 0.5$, $n = 1.0$

5.3 Small-scale parameter effect

Figure 3a–c shows the small-scale effects on the nonlinear time history of the dimensionless midpoint deflection of PSDBT model for C–C, C–S and S–S boundary conditions, respectively. It is seen from Fig. 3 that increasing small-scale parameter decreases the maximum midpoint dimensionless deflection for different boundary conditions. It is due to the fact that according to Eqs. (1) and (8) increasing the small-scale parameter increases the strain energy of the system which yields reduction in dimensionless deflection of the FGMSNB. Moreover, the effect of small-scale parameter becomes more distinguished for C–C boundary conditions. Furthermore, comparing the dimensionless midpoint

deflection values shows that the C–C end conditions yield lower deflection in comparison with other boundary conditions. Therefore, the obtained numerical results are consistent with physical results where the stiffer boundary conditions yields lower deflections. It should be mentioned that for the following sections, the $l = 0.2h_l$ is selected for the small-scale parameter unless otherwise mentioned.

5.4 Geometrical parameters effect

In order to show the effects of geometrical parameters on the nonlinear midpoint deflection of the FGMSNB, Figs. 4 and 5 are plotted for different boundary conditions. To this purpose in the present section, the small-scale parameter is chosen $l = 0.3$ (nm). In order to show the effect of magnetostrictive layers thickness on the dimensionless midpoint deflection, Fig. 4 is plotted for C–C FGMSNB with $L = 12$ (nm). It is seen from Fig. 4 that increasing the thickness of magnetostrictive layers decreases the midpoint deflection of the nanobeam. From the physically point of view, with increasing the thickness of magnetostrictive layers the bending rigidity of FGMSNB increases, therefore, the deflection should be decreased. Therefore, the numerical results match the physical results.

In Fig. 5, the length effect of the FGMSNB on the time history of the dimensionless midpoint deflection is plotted. From Fig. 5, it is observed that increasing the length of the FGMSNB decreases the midpoint deflection. Therefore, increasing the length of the FGMSNB decreases the stability of the system.

5.5 Effect of environment temperature

To evaluate the influence of environment temperature on the midpoint deflection of the nanobeam for both linear and nonlinear solutions and C–C, C–S and S–S boundary conditions, Fig. 6 is plotted. From Fig. 6, it can be observed that the dimensionless midpoint deflection of the FGMSNB increases with increasing the environment temperature for both linear and nonlinear solutions and different boundary conditions. It is due to this fact that increasing the environment temperature makes the system looser which yields an increase in deflection of the system. Therefore, the effect of environment temperature on the properties of the FGM core should not be neglected in dynamic analysis. Also, the dimensionless midpoint deflections from linear solution are higher than those obtained from nonlinear solution. From Eqs. (12) and (14), it can be obtained that considering nonlinear terms increases the strain energy of the system. Therefore, the dimensionless deflections obtained from nonlinear solution should be lower than those obtained from linear solution.

Table 2 Maximum values of dimensionless midpoint deflection for different number of grid points for C–C boundary conditions

Theory	$N = 5$	$N = 7$	$N = 9$	$N = 11$	$N = 13$	$N = 15$	$N = 17$
<i>FSDBT</i>							
Linear	0.691	0.697	0.692	0.694	0.695	0.694	0.694
Nonlinear	0.616	0.619	0.620	0.619	0.621	0.620	0.620
<i>PSDBT</i>							
Linear	0.691	0.698	0.693	0.695	0.696	0.695	0.695
Nonlinear	0.616	0.620	0.620	0.620	0.621	0.621	0.621
<i>TSDBT</i>							
Linear	0.693	0.698	0.693	0.695	0.696	0.695	0.695
Nonlinear	0.615	0.619	0.620	0.620	0.621	0.621	0.621
<i>HSDBT</i>							
Linear	0.691	0.698	0.693	0.695	0.696	0.695	0.695
Nonlinear	0.616	0.620	0.620	0.620	0.621	0.621	0.621
<i>ESDBT</i>							
Linear	0.691	0.697	0.692	0.694	0.695	0.694	0.694
Nonlinear	0.616	0.619	0.620	0.619	0.621	0.620	0.620

5.6 Surrounding elastic medium effect

Figures 7, 8 and 9 depict the effect of Winkler, Pasternak and visco-Pasternak elastic mediums, respectively, on the time history of the FGSNB nonlinear midpoint deflection. As can be seen, increasing each parameter of elastic medium such as spring, shear and damping constants of elastic medium decreases the midpoint dynamic deflection at a decreasing rate for different boundary conditions. Furthermore, increasing the damping modulus of elastic medium increases the period of midpoint deflection oscillations.

5.7 Influence of magnetostrictive layers

Figure 10 illustrates the effect of magnetostrictive layers on the nonlinear midpoint dimensionless deflection for C–C, C–S and S–S boundary conditions, respectively. It is seen that increasing the velocity feedback gain ($k_{c,c}(t)$) decreases the dimensionless midpoint deflection for different boundary conditions. Moreover, it can be concluded from Fig. 10 that the effect of velocity feedback gain is more prominent for S–S boundary conditions than others. Also, the effect of velocity feedback gain becomes more evident in results obtained from nonlinear solution.

Table 3 Maximum values of dimensionless midpoint deflection for different number of grid points for C–S boundary conditions

Theory	$N = 5$	$N = 7$	$N = 9$	$N = 11$	$N = 13$	$N = 15$	$N = 17$	$N = 19$	$N = 21$
<i>FSDBT</i>									
Linear	0.979	0.975	0.967	0.981	0.993	0.997	0.997	0.997	0.997
Nonlinear	0.771	0.766	0.763	0.763	0.762	0.767	0.771	0.773	0.773
<i>PSDBT</i>									
Linear	0.980	0.976	0.968	0.980	0.992	0.996	0.997	0.996	0.996
Nonlinear	0.771	0.766	0.763	0.763	0.762	0.766	0.771	0.773	0.773
<i>TSDBT</i>									
Linear	0.980	0.976	0.967	0.979	0.992	0.996	0.996	0.996	0.996
Nonlinear	0.772	0.766	0.763	0.763	0.762	0.766	0.770	0.773	0.773
<i>HSDBT</i>									
Linear	0.980	0.976	0.968	0.980	0.992	0.996	0.997	0.996	0.996
Nonlinear	0.771	0.766	0.763	0.763	0.762	0.766	0.771	0.773	0.773
<i>ESDBT</i>									
Linear	0.979	0.975	0.967	0.981	0.993	0.997	0.997	0.997	0.997
Nonlinear	0.771	0.766	0.763	0.763	0.762	0.767	0.771	0.773	0.773

Table 4 Maximum values of dimensionless midpoint deflection for different number of grid points for S–S boundary conditions

Theory	$N = 5$	$N = 7$	$N = 9$	$N = 11$	$N = 13$	$N = 15$
<i>FSDBT</i>						
Linear	1.543	1.418	1.422	1.422	1.422	1.422
Nonlinear	1.041	0.921	0.921	0.920	0.920	0.920
<i>PSDBT</i>						
Linear	1.543	1.418	1.422	1.422	1.422	1.422
Nonlinear	1.041	0.921	0.921	0.920	0.921	0.921
<i>TSDBT</i>						
Linear	1.543	1.419	1.422	1.422	1.422	1.422
Nonlinear	1.041	0.921	0.921	0.920	0.920	0.920
<i>HSDBT</i>						
Linear	1.543	1.419	1.422	1.422	1.422	1.422
Nonlinear	1.041	0.921	0.921	0.920	0.921	0.921
<i>ESDBT</i>						
Linear	1.543	1.418	1.422	1.422	1.422	1.422
Nonlinear	1.041	0.921	0.921	0.920	0.920	0.920

5.8 Influence of material composition of the core

Figure 11 depicts the effect of material composition of the core layer by illustrating the variation of nonlinear dimensionless midpoint deflection versus the dimensionless time for different boundary conditions. It can be concluded for different boundary conditions, increasing the power law exponent leads to increasing the dimensionless midpoint deflection at a decreasing rate.

6 Conclusion

Due to this fact that, dynamic analysis of nanobeam has been attracted much attention in NEMS, in this study the nonlinear dynamic analysis of FGMSNBs embedded in visco-Pasternak foundation was investigated using different beam models. The MCST was utilized to study the effect of small-scale parameter on the deflection of the nanobeam. Energy method and Hamilton's principle were taken into account to obtain the governing motion equations and related boundary conditions. The results of this study were validated as far as possible with those obtained by Rao [25] and the influences of small-scale effect, geometrical parameters, environment temperature, surrounding elastic medium, magnetostrictive layers, material composition of core layer and boundary conditions were studied in detail. The obtained results would be beneficial for the design of sensors and actuators in NEMS. The following conclusions were made from the results:

1. Results obtained from different theories are close to each other; therefore, the PSDBT theory had been taken into consideration.
2. The dynamic response of the SNB is significantly influenced by the small-scale effect; increasing small-scale parameter decreases the maximum midpoint dimensionless deflection for different boundary conditions. Therefore, neglecting small-scale effects leads to inaccurate results.
3. Comparing results from different boundary conditions shows that the midpoint deflection for S–S boundary conditions is higher than those obtained from C–C and C–S boundary conditions.
4. Midpoint deflection values obtained from nonlinear solution are lower than those obtained from linear solution. It is due to the fact that considering nonlinear terms increases the strain energy of the system.
5. Increasing the velocity feedback gain increases the dimensionless deflection of the FGSNB.

Appendix A

Equations (30) can be written as the following form:

$$[\bar{M}]\{\ddot{d}\} + [\bar{C}_{NL} + \bar{C}_L]\{\dot{d}\} + [\bar{K}_{NL} + \bar{K}_L]\{d\} = \{\bar{F}\}, \quad (34)$$

in which $[\bar{M}]$ is the mass matrix, $[\bar{C}_{NL} + \bar{C}_L]$ are the nonlinear and linear damping matrixes, $[\bar{K}_{NL} + \bar{K}_L]$ are the nonlinear and linear stiffness matrixes and $\{\bar{F}\}$ is the harmonically varying load matrix and:

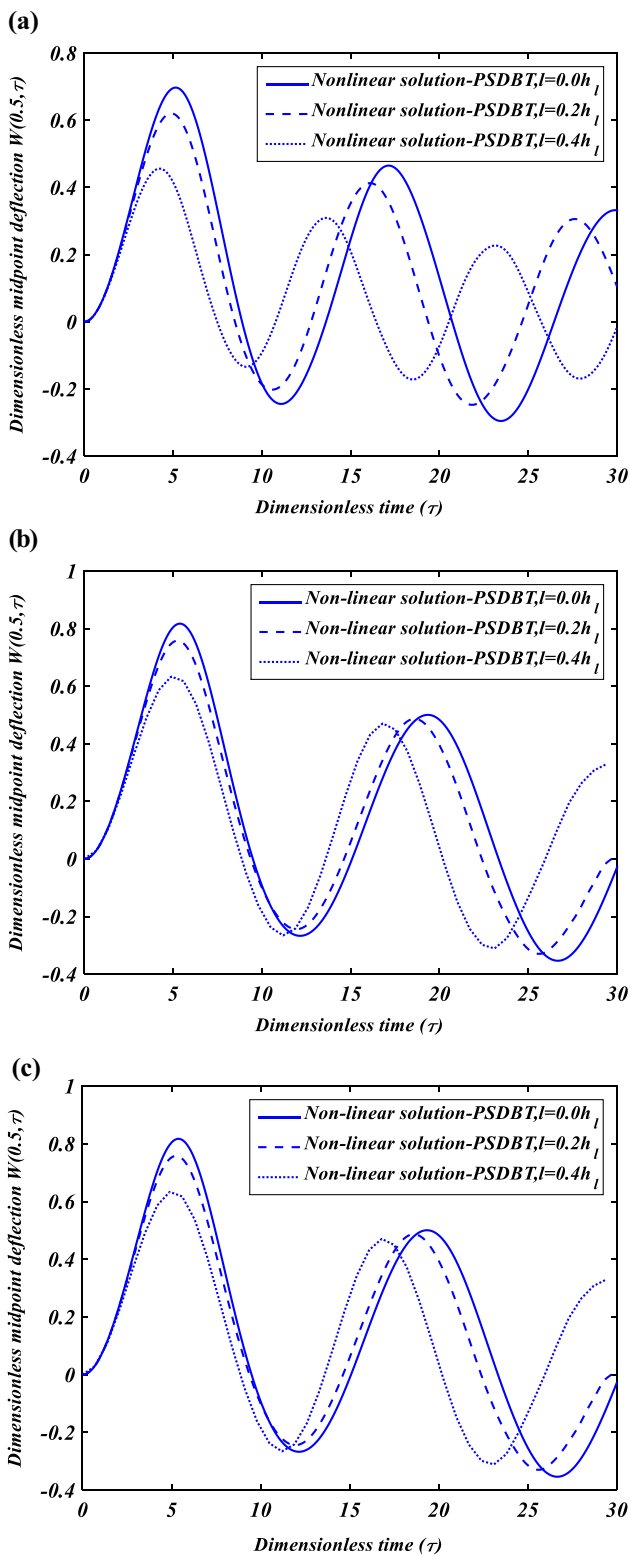


Fig. 3 Small-scale effect on the time history of midpoint dimensionless deflection **a** C–C, **b** C–S and **c** S–S

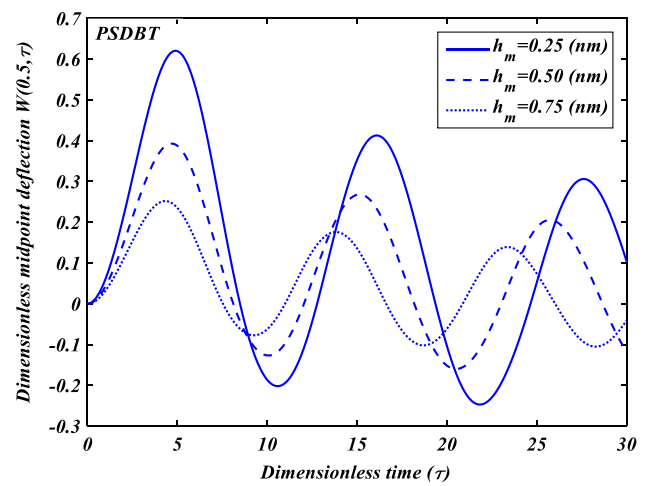


Fig. 4 Magnetostrictive layers thickness effect on the time history of midpoint dimensionless deflection

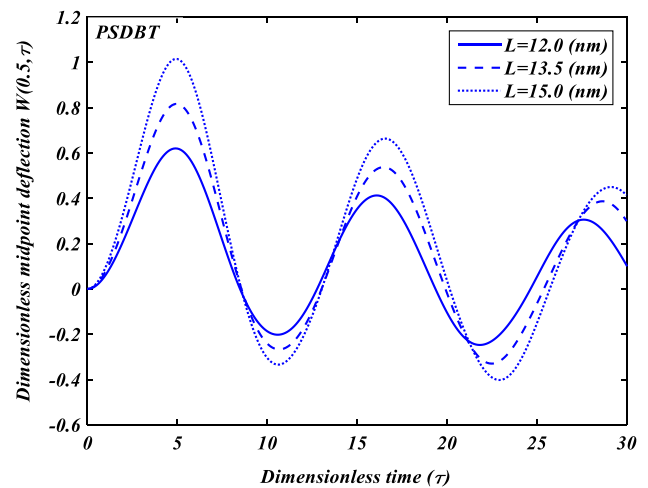


Fig. 5 FGSNB length effect on the time history of midpoint dimensionless deflection

$$\{d\} = \left\{ \{U_i\}^T, \{W_i\}^T, \{\Gamma_i\}^T \right\}. \tag{35}$$

On the other hand, Eqs. (31) can be rewritten as follows:

$$[B]\{d\} = \{S\}, \tag{36}$$

where $[B]$ and $\{S\}$ are stiffness and nonhomogeneous terms of boundary conditions.

Separation of boundary and domain points of Eq. (36) yields:

$$[B]_b\{d\}_b + [B]_d\{d\}_d = \{S\}, \tag{37}$$

From Eq. (37), the following equation can be obtained:

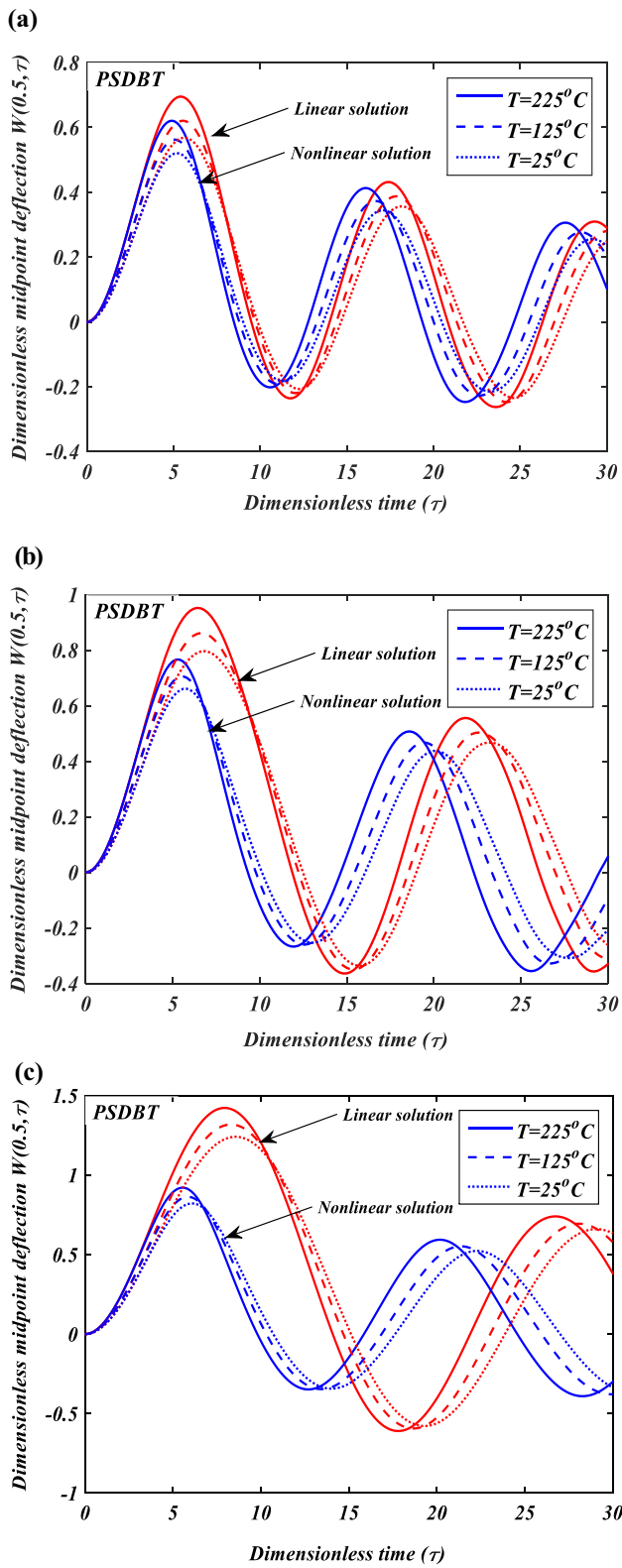


Fig. 6 Environment temperature effect on the time history of midpoint dimensionless deflection a C-C, b C-S and c S-S

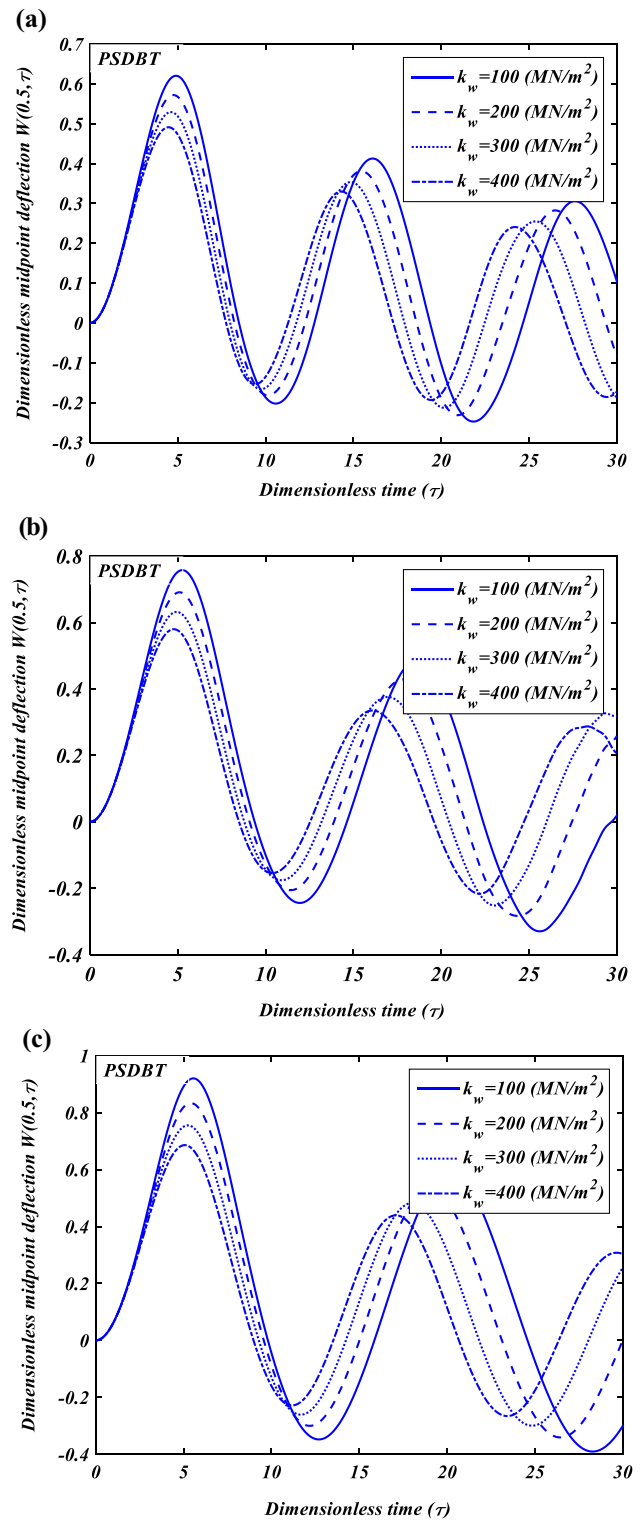


Fig. 7 Winkler constant of elastic medium effect on the time history of midpoint dimensionless deflection a C-C, b C-S and c S-S

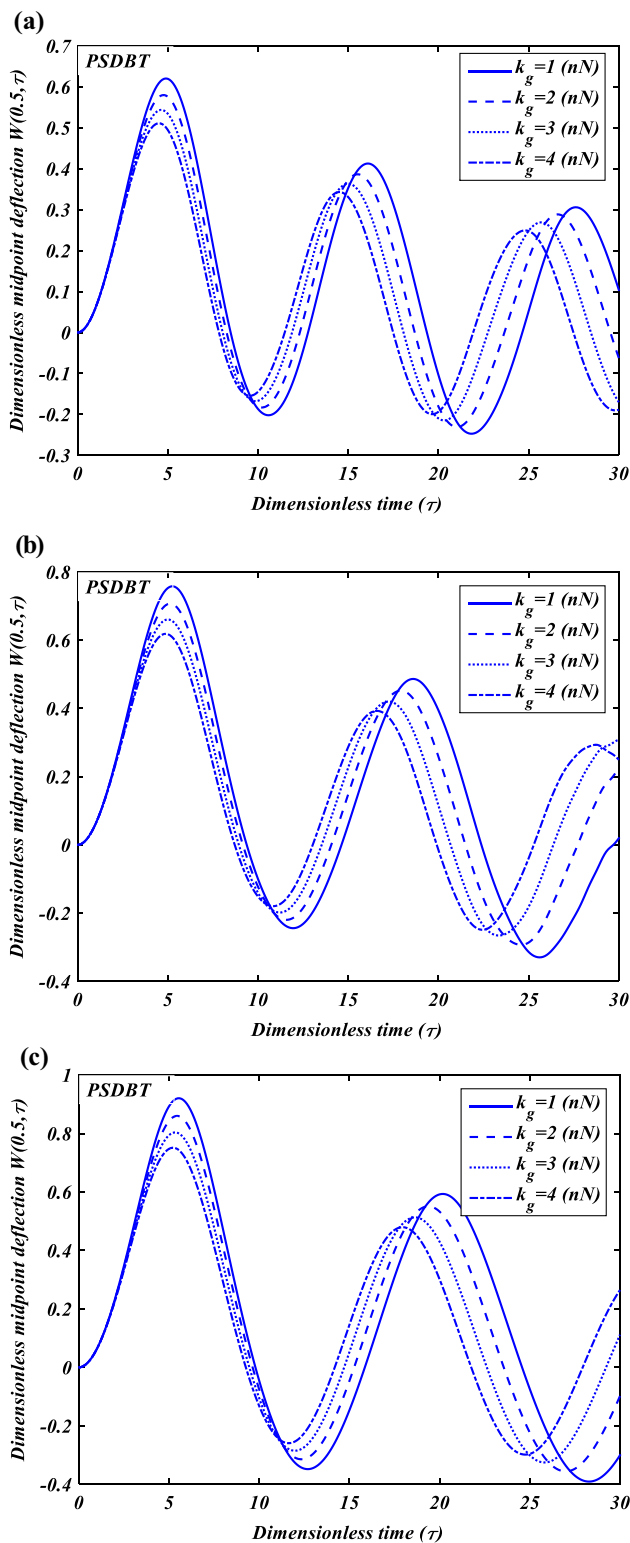


Fig. 8 Pasternak constant of elastic medium effect on the time history of midpoint dimensionless deflection **a** C-C, **b** C-S and **c** S-S

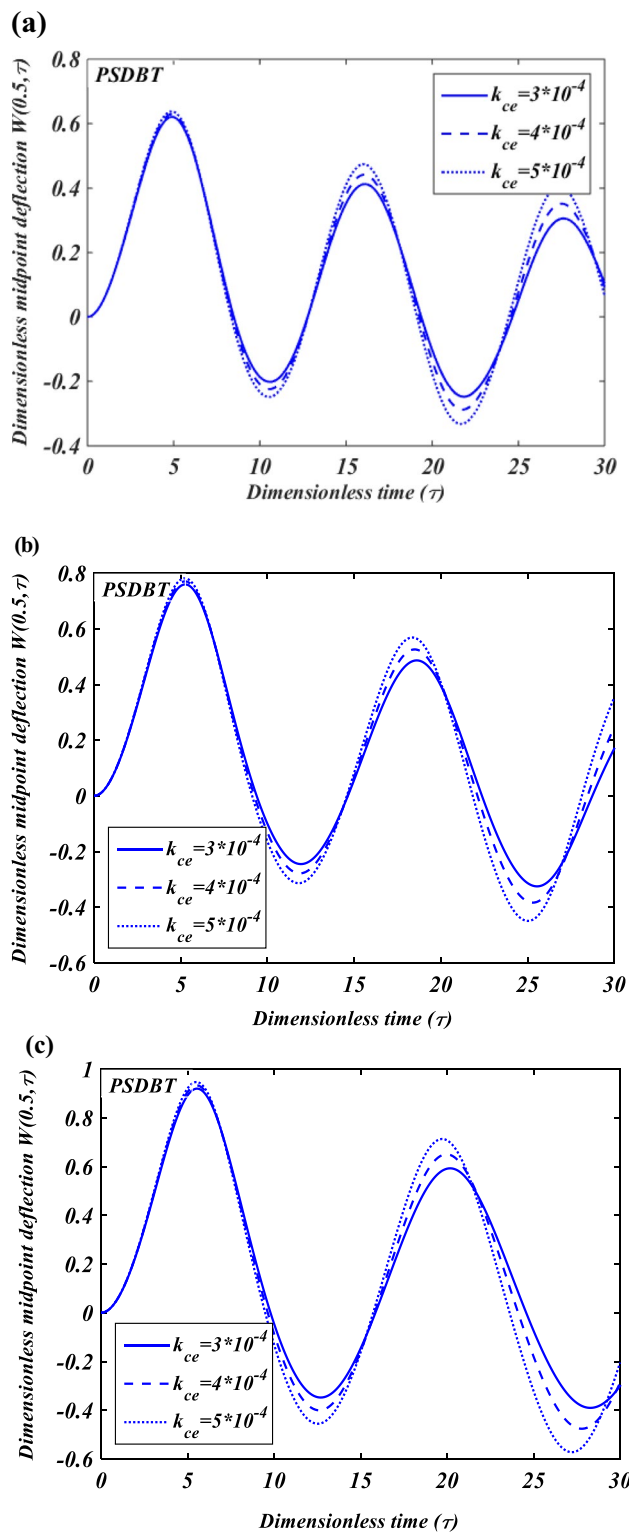


Fig. 9 Damping constant of elastic medium effect on the time history of midpoint dimensionless deflection **a** C-C, **b** C-S and **c** S-S

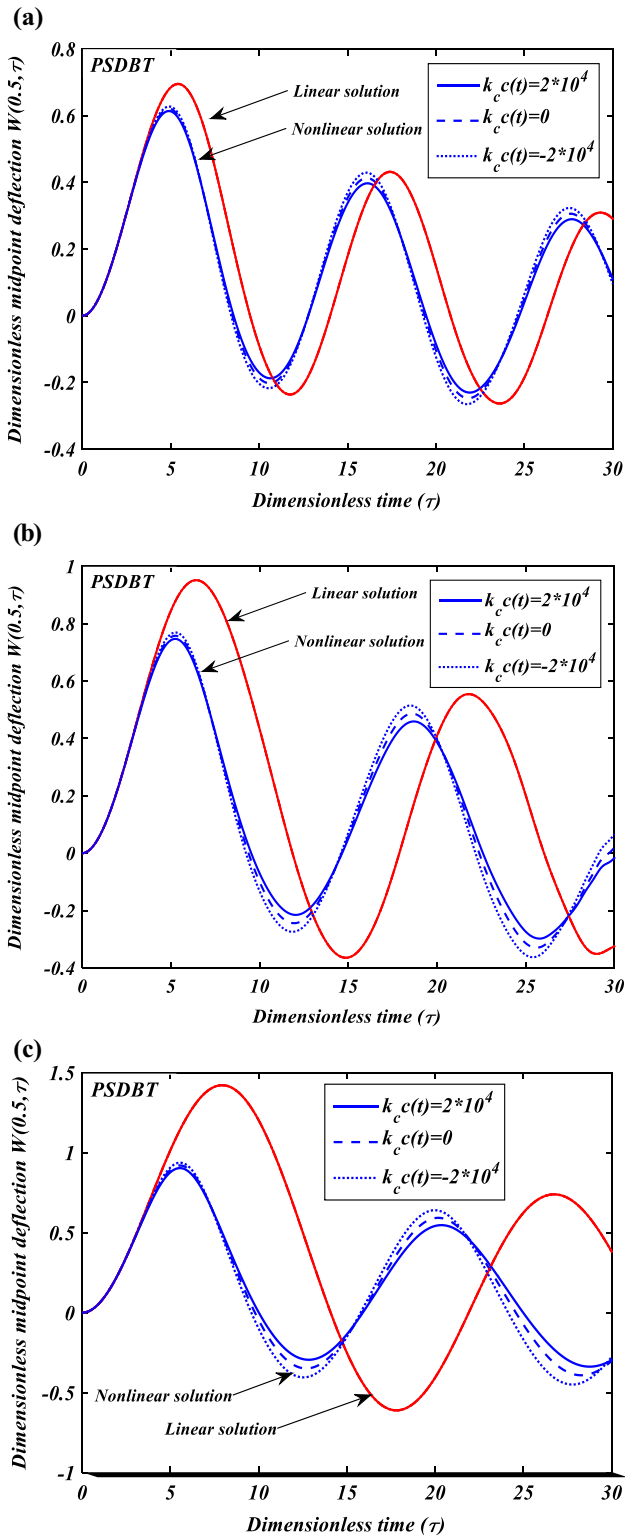


Fig. 10 Effects of magnetostrictive layers on the midpoint dimensionless longitudinal displacement **a** C–C, **b** C–S and **c** S–S

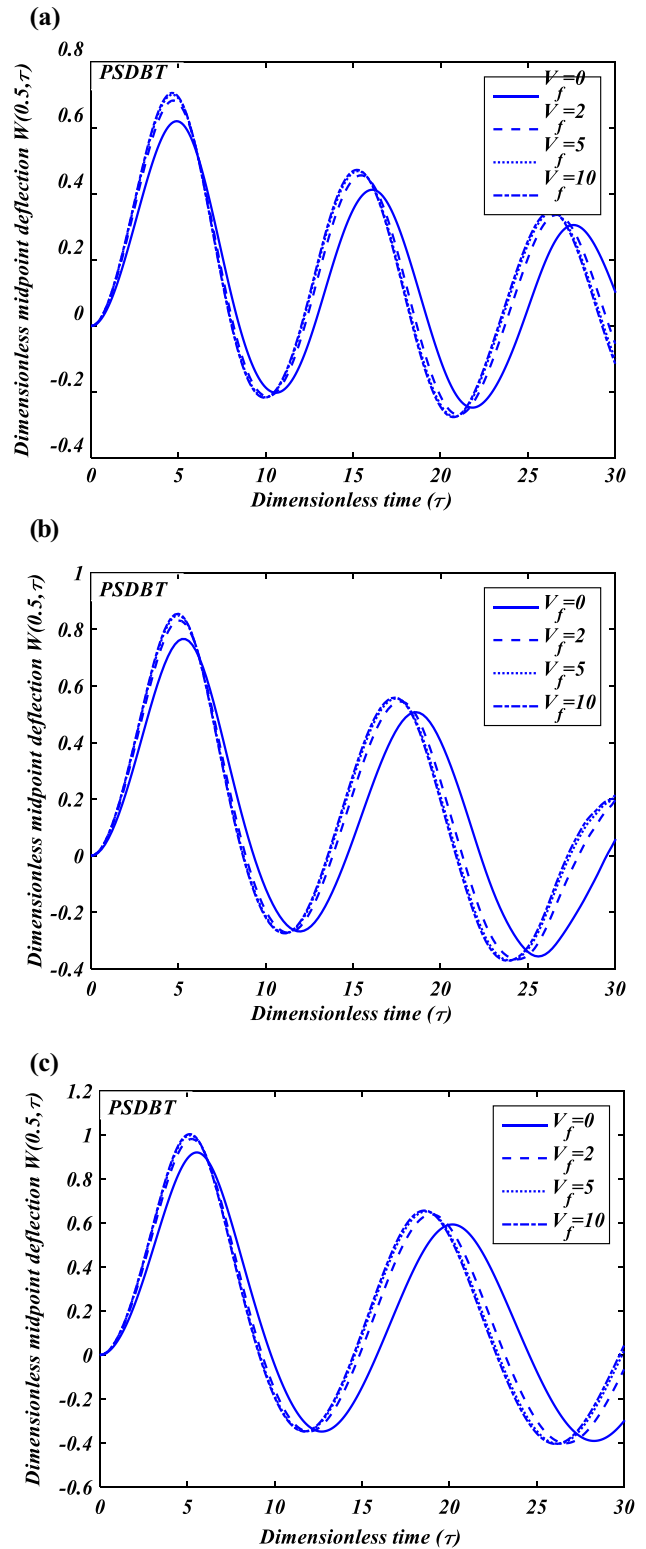


Fig. 11 Effects of materials composition of core layer on the midpoint dimensionless longitudinal displacement **a** C–C, **b** C–S and **c** S–S

$$\{d\}_b = [B]_b^{-1}\{S\} - [B]_b^{-1}[B]_d\{d\}_d, \quad (38)$$

Therefore:

$$\{\dot{d}\}_b = -[B]_b^{-1}[B]_d\{\dot{d}\}_d, \quad (39)$$

$$\{\ddot{d}\}_b = -[B]_b^{-1}[B]_d\{\ddot{d}\}_d, \quad (40)$$

Omitting rows related to boundary points in Eq. (34) yields the following equation as:

$$[\tilde{M}]\{\ddot{d}\} + [\tilde{C}_{NL} + \tilde{C}_L]\{\dot{d}\} + [\tilde{K}_{NL} + \tilde{K}_L]\{d\} = \{\tilde{F}\}, \quad (41)$$

Similarly, separating boundary and domain points in Eq. (41) yields:

$$\begin{aligned} & [\tilde{M}]_b\{\ddot{d}\}_b + [\tilde{M}]_d\{\ddot{d}\}_d + [\tilde{C}_{NL}]_b\{\dot{d}\}_b \\ & + [\tilde{C}_{NL}]_d\{\dot{d}\}_d + [\tilde{C}_L]_b\{\dot{d}\}_b + [\tilde{C}_L]_d\{\dot{d}\}_d + \\ & + [\tilde{K}_{NL}]_b\{d\}_b + [\tilde{K}_{NL}]_d\{d\}_d + [\tilde{K}_L]_b\{d\}_b \\ & + [\tilde{K}_L]_d\{d\}_d = \{\tilde{F}\}, \end{aligned} \quad (42)$$

Substituting Eqs. (38), (39) and (40) into Eq. (42) yields the following equation as:

$$[M]\{\ddot{d}\}_d + [C_{NL} + C_L]\{\dot{d}\}_d + [K_{NL} + K_L]\{d\}_d = \{F\}, \quad (43)$$

where

$$[M] = [\tilde{M}]_d - [\tilde{M}]_b[B]_b^{-1}[B]_d, \quad (44)$$

$$[C_L] = [\tilde{C}_L]_d - [\tilde{C}_L]_b[B]_b^{-1}[B]_d, \quad (45)$$

$$[C_{NL}] = [\tilde{C}_{NL}]_d - [\tilde{C}_{NL}]_b[B]_b^{-1}[B]_d, \quad (46)$$

$$[K_L] = [\tilde{K}_L]_d - [\tilde{K}_L]_b[B]_b^{-1}[B]_d, \quad (47)$$

$$[K_{NL}] = [\tilde{K}_{NL}]_d - [\tilde{K}_{NL}]_b[B]_b^{-1}[B]_d, \quad (48)$$

$$[F] = [\tilde{F}]_d - [\tilde{K}_L]_b[B]_b^{-1}\{S\} - [\tilde{K}_{NL}]_b[B]_b^{-1}\{S\}, \quad (49)$$

References

- Wang Q, Lin M (2017) Design of new giant magnetostrictive structures for double-nut ball screw pre-tightening. *J Braz Soc Mech Sci* 39:3181–3188
- Yongping W, Daining F, Soh AK, Hwang KC (2003) Experimental and theoretical study of the nonlinear response of a giant magnetostrictive rod. *Acta Mech Sci* 19:324–329
- Dai L, Jazar RN (2018) *Nonlinear Approaches in Engineering Applications*. Springer
- Mishra H, Chelvane JA, Arockiarajan A (2017) Influence of a thermal environment on the deflection of magnetostrictive thin films. *Acta Mech* 228:1909–1921
- Ebrahimi F, Dabbagh A (2018) Thermo-magnetic field effects on the wave propagation behavior of smart magnetostrictive sandwich nanoplates. *Eur Phys J Plus* 133:97
- Kumar JS, Ganesan N, Swarnamani S, Padmanabhan C (2003) Active control of beam with magnetostrictive layer. *Comput Struct* 81:1375–1382
- Fu Y, Wang J, Mao Y (2012) Nonlinear analysis of buckling, free vibration and dynamic stability for the piezoelectric functionally graded beams in thermal environment. *Appl Math Model* 36:4324–4340
- Fallah A, Aghdam MM (2012) Thermo-mechanical buckling and nonlinear free vibration analysis of functionally graded beams on nonlinear elastic foundation. *Compos Part B Eng* 43:1523–1530
- Li SR, Batra RC (2013) Relations between buckling loads of functionally graded Timoshenko and homogeneous Euler-Bernoulli beams. *Compos Struct* 95:5–9
- Shen HS, Wang ZX (2014) Nonlinear analysis of shear deformable FGM beams resting on elastic foundations in thermal environments. *Int J Mech Sci* 81:195–206
- Bui TQ, Khosravifard A, Zhang CH, Hematiyan MR, Golub MV (2013) Dynamic analysis of sandwich beams with functionally graded core using a truly meshfree radial point interpolation method. *Eng Struct* 47:90–104
- Pradeep V, Ganesan N, Bhaskar K (2007) Vibration and thermal buckling of composite sandwich beams with viscoelastic core. *Compos Struct* 81:60–69
- Yang Y, Lam CC, Kou KP, Iu VP (2014) Free vibration analysis of the functionally graded sandwich beams by a meshfree boundary-domain integral equation method. *Compos Struct* 117:32–39
- Vo TP, Thai HT, Nguyen TK, Mazaheri A, Lee J (2014) Finite element model for vibration and buckling of functionally graded sandwich beams based on a refined shear deformation theory. *Eng Struct* 64:12–22
- Simsek M, Reddy JN (2013) Bending and vibration of functionally graded microbeams using a new higher order beam theory and the modified couple stress theory. *Int J Eng Sci* 64:37–53
- Fakhrabadi MMS, Yang J (2015) Comprehensive nonlinear electromechanical analysis of nanobeams under DC/AC voltages based on consistent couple-stress theory. *Compos Struct* 132:1206–1218
- Simsek M (2014) Nonlinear static and free vibration analysis of microbeams based on the nonlinear elastic foundation using modified couple stress theory and He's variational method. *Compos Struct* 112:264–272
- Akgoz B, Civalek O (2011) Strain gradient elasticity and modified couple stress models for buckling analysis of axially loaded micro-scaled beams. *Int J Eng Sci* 49:1268–1280
- Ghorbanpour Arani A, Shokravi M (2015) Vibration response of visco-elastically coupled double-layered visco-elastic graphene sheet systems subjected to magnetic field via strain gradient theory considering surface stress effects. *Proc Inst Mech Eng N J Nanoeng Nanosyst*. <https://doi.org/10.1177/1740349914529102>
- Ghorbanpour Arani A, Kolahchi R, Zarei MSh (2015) Visco-surface-nonlocal piezoelectricity effects on nonlinear dynamic stability of graphene sheets integrated with ZnO sensors and actuators using refined zigzag theory. *Compos Struct* 132:506–523
- Ghorbanpour Arani A, Abdollahian M (2017) Transient response of FG higher-order nanobeams integrated with magnetostrictive layers using modified couple stress theory. *Mech Adv Mater Struct*. <https://doi.org/10.1080/15376494.2017.1387326>
- Ghorbanpour Arani A, Abdollahian M, Kolahchi R (2015) Nonlinear vibration of embedded smart composite microtube conveying

- fluid based on modified couple stress theory. *Polym Compos* 36:1314–1324
23. Ghorbanpour Arani A, Abdollahian M, Jalaei MH (2015) Vibration of bioliquid-filled microtubules embedded in cytoplasm including surface effects using modified couple stress theory. *J Theor Biol* 367:29–38
 24. Pradhan SC (2005) Vibration suppression of FGM shells using embedded magnetostrictive layers. *Int J Solids Struct* 42:2465–2488
 25. Singiresu SR (2007) *Vibration of continuous systems*. Wiley, New York
 26. Ke LL, Wang YS (2014) Free vibration of size-dependent magneto-electro-elastic nanobeams based on the nonlocal theory. *Physica E* 63:52–61

Publisher's Note Springer Nature remains neutral with regard to jurisdictional claims in published maps and institutional affiliations.